Liquid Crystals
Publication details, including instructions for authors and subscription information:
http://www.informaworld.com/smpp/title~content=t713926090

A tensor model of liquid crystalline polymers: application to basic disclination processes

Houjie Tu; Gerhard Goldbeck-Wood; Alan H. Windle

Online publication date: 11 November 2010

To cite this Article Tu, Houjie , Goldbeck-Wood, Gerhard and Windle, Alan H.(2002) 'A tensor model of liquid crystalline polymers: application to basic disclination processes', Liquid Crystals, 29: 3, 325 — 334
To link to this Article: DOI: 10.1080/02678290110098647
URL: http://dx.doi.org/10.1080/02678290110098647

LIQUID CRYSTALS, 2002, VOL. 29, NO. 3, 325–334

Taylor & Francis
Taylor & Francis Group

A tensor model of liquid crystalline polymers: application to basic disclination processes

HOUJIE TU, GERHARD GOLDBECK-WOOD† and ALAN H. WINDLE*
Department of Materials Science and Metallurgy, University of Cambridge, Cambridge CB2 3QZ, UK

(*Received 12 May 2001; accepted 29 June 2001*)

One of the features of liquid crystalline polymers (LCPs) is their strong elastic anisotropy, which means they have unequal elastic constants. Elastic anisotropy plays a crucial role in the microstructure and macroscopic properties of LCPs. In this paper, the effect of unequal elastic constants on microstructure is investigated without an external field by using a deterministic tensorial approach. In this model, the evolution of the director field can be viewed as a process driven towards the state of zero elastic torque. A tensor expression of the elastic torque is used so that the nematic symmetry is automatically conserved. In simulations of bulk samples, disclination lines of strength half and escaped integer disclinations are observed. The distortion fields around the disclinations are found to depend on elastic anisotropy. If the twist constant is the lowest, as is the case for main chain liquid crystalline polymers, the disclination lines are predominantly of the twist type.

1. Introduction

Spatial inhomogeneity of the director field **n** plays an important role in a highly textured nematic liquid crystalline polymer (LCP). The distortion of the director can be described by the Frank elastic free energy, which has three components: splay, twist and bend, with respective elastic constants [1]. Compared with small molecular weight liquid crystals (SMWLCs), LCPs have strong elastic anisotropy [2], i.e. the three elastic constants have significantly different values. For example, for main chain thermotropic LCPs, the splay elastic constant is considerably greater than the bend and twist elastic constants, since the concentration of the chain ends is low [3, 4].

For SMWLCs, the three elastic constants can be determined by the Fréedericksz transitions [1] or a light scattering technique [5]. Unfortunately, the measurement methods of the three elastic constants for SMWLCs are not applicable to LCPs since uniformly oriented specimens of LCPs are hardly ever obtained. On the other hand, for SMWLCs, the observation of the microstructures corresponding to the various optical textures is difficult to handle because the specimens are in the liquid state. For LCPs, the long relaxation time due to the long chain structure provides a possibility of investigating the microstructures by quenching the samples into a glassy phase [6–8]. Elastic anisotropy for a thermotropic copolyester was determined by measuring the distortion around a wedge disclination decorated by lamellar structure [9]. However, in a recent study, it was found that this method was undermined by neighbouring disclination interactions, and should be applied only to a completely isolated disclination [10]. Therefore, a systematic measurement of the elastic constants for LCPs is still a challenge. The study of the influence of elastic anisotropy on the microstructure is mostly confined to a theoretical field [11–12]. It is believed that elastic anisotropy has considerable influence on the microstructure and macroscopic properties of LCPs [1, 2]. The single-constant assumption is not appropriate for long chain liquid crystalline systems.

In numerical simulations, most previous treatments assumed equal constants to simplify the calculation. The exceptions were some recent Monte Carlo based simulations for tackling the unequal elastic constants issue [13–16]. In these models, an LCP was represented by a set of directors **n** on a spatially fixed cubic lattice. The relaxation algorithms were designed to minimize the total free energy of the system. To calculate the free energy of a cell, the vectorial and tensorial forms of the Frank free energy were used, respectively. In [14], the nematic symmetry, which means that **n** and $-\mathbf{n}$ are equivalent, was treated by a flip vectorial scheme.

*Author for correspondence; e-mail: ahw1@cus.cam.ac.uk
†Present address: Accelrys Ltd., The Quorum, Cambridge CB5 8RE, UK.

Liquid Crystals ISSN 0267-8292 print/ISSN 1366-5855 online © 2002 Taylor & Francis Ltd
http://www.tandf.co.uk/journals
DOI: 10.1080/02678290110098647

In a previous paper [17], we presented a deterministic model dealing with the three Frank elastic constants. According to this model, the evolution of the directors could be considered as finding the state in which the directors were parallel to the 'texture field', instead of finding the minimum of the elastic free energy. The elastic effect of the textures was taken into account by using a tensor expression of the elastic torque, in which the three elastic constants were included and nematic symmetry was conserved automatically. The simulation results of the Fréedericksz transitions were in perfect agreement with the analytical solutions [17].

In the current paper, this model is used for simulations of the disclination structure for a range of elastic anisotropies both in 2D and 3D. A brief description of the governing equations and numerical model is given in § 2; details can be found in [17]. In § 3 and § 4, the simulation results of the annealing of defects in a planar and a bulk sample, respectively, are given. Finally, § 5 summarizes this investigation.

2. Numerical model

The Frank elastic free energy can be written in the following tensorial form [13]

$$f = \frac{1}{2}\left[\frac{1}{2}k_2 \nabla_\lambda n_\mu n_\nu \nabla_\lambda n_\mu n_\nu + (k_1 - k_2)\nabla_\lambda n_\lambda n_\mu \nabla_\nu n_\nu n_\mu + \frac{1}{2}(k_3 - k_1) n_\mu n_\nu \nabla_\mu n_\lambda n_\kappa \nabla_\nu n_\lambda n_\kappa \right] \quad (1)$$

where $\mathbf{n}$ is the director, $\mathbf{n}\ \mathbf{n} = 1$ and $\mathbf{n}$ is equivalent to $-\mathbf{n}$; k_1, k_2 and k_3 are the three Frank elastic constants which are associated with the three types of deformations, splay, twist and bend, respectively.

Equation (1) is equivalent to the vectorial form of the Frank elastic free energy except for the surface terms [12]. The Greek subscripts refer to the Cartesian components, and

$$\nabla_\alpha = \frac{\partial}{\partial x_\alpha}, \quad \mathbf{r} = (x_1, x_2, x_3) = (x, y, z).$$

The summation convention is used.

The equation of motion for director relaxation has the following form,

$$\frac{\partial \mathbf{n}}{\partial t} = \frac{1}{\gamma_1}(\mathbf{n} \times \mathbf{h}) \times \mathbf{n} \quad (2)$$

where $\mathbf{n} \times \mathbf{h}$ is the torque per unit volume due to the curvature elasticity, and γ_1 is the rotational viscous coefficient. The 'texture field', $\mathbf{h}$, which emanates from spatial director inhomogeneity, is found to take the following form [17]:

$$h_\beta = 2n_\alpha \left\{ k_2 \Delta n_\alpha n_\beta + (k_1 - k_2) \times \left[\nabla_{\alpha\gamma} n_\gamma n_\beta + \nabla_{\beta\gamma} n_\gamma n_\alpha - \frac{2}{3}\delta_{\alpha\beta} \nabla_{\gamma\lambda} n_\gamma n_\lambda \right] + (k_3 - k_1)\left[\nabla_\gamma (n_\gamma n_\lambda \nabla_\lambda n_\alpha n_\beta) - \frac{1}{2}\nabla_\alpha n_\gamma n_\lambda \nabla_\beta n_\gamma n_\lambda + \frac{1}{6}\delta_{\alpha\beta} \nabla_\gamma n_\lambda n_\mu \nabla_\gamma n_\lambda n_\mu \right] \right\} \quad (3)$$

where

$$\nabla_{\alpha\beta} = \frac{\partial^2}{\partial x_\alpha \partial x_\beta}.$$

In the equilibrium state, the director $\mathbf{n}$ must be, at each point, parallel to the 'texture field'.

Equations (2) and (3) describe the relaxation behaviour of the director field. For a given initial pattern and boundary conditions, equation (2) can be integrated numerically by standard techniques.

The nematic is represented by a set of directors on a spatially fixed cubic lattice. A normal finite difference scheme is adopted for discretizing equation (2) on this lattice. Starting from the given director pattern and boundary conditions, the evolution of the director in each cell can be described by the following equation

$$n_\beta^{\text{new}} = n_\beta^{\text{old}} + \frac{\Delta t}{\gamma_1}(h_\beta^{\text{old}} - n_\alpha^{\text{old}} h_\alpha^{\text{old}} n_\beta^{\text{old}}). \quad (4)$$

Here Δt is the time step, $\beta = 1, 2, 3$. n_β^{old} and n_β^{new} are the directors at the previous time step and the current time step, respectively. h_β^{old} can be calculated by discretizing equation (3).

3. Director annealing in thin films

If the directors are constrained to lie in a plane, as is the case in thin films, distortions are restricted to bend and splay, i.e. the twist distortion is forbidden. Therefore distortions in two dimensions are of pure wedge character [1]; these correspond to the Schlieren texture in a thin nematic specimen observed by polarizing optical microscopy. The 2D version of the model [17] can hence be used to simulate the structures of wedge disclinations and the effect of splay and bend elastic anisotropy on them.

Starting from an isotropic phase, the annealing procedure can be described as follows. Randomly oriented directors tend to form half strength defect pairs. At the beginning of annealing, a large number of defects with half strength are generated. The number of $+1/2$ defects is always equal to the number of $-1/2$ defects, as the

analytic result predicted [1, 2]. Defect pairs of opposite strength tend to attract each other and finally annihilate, in order to reduce the elastic torque. This leads to the decrease of the defect density corresponding to the texture coarsening observed in experiments [18]. In the current deterministic model, the system is driven towards a state of zero elastic torque. Sometimes a mono-domain configuration is reached, corresponding to the global minimum free energy state. However, it is also possible that a state of zero torque is reached with some defect

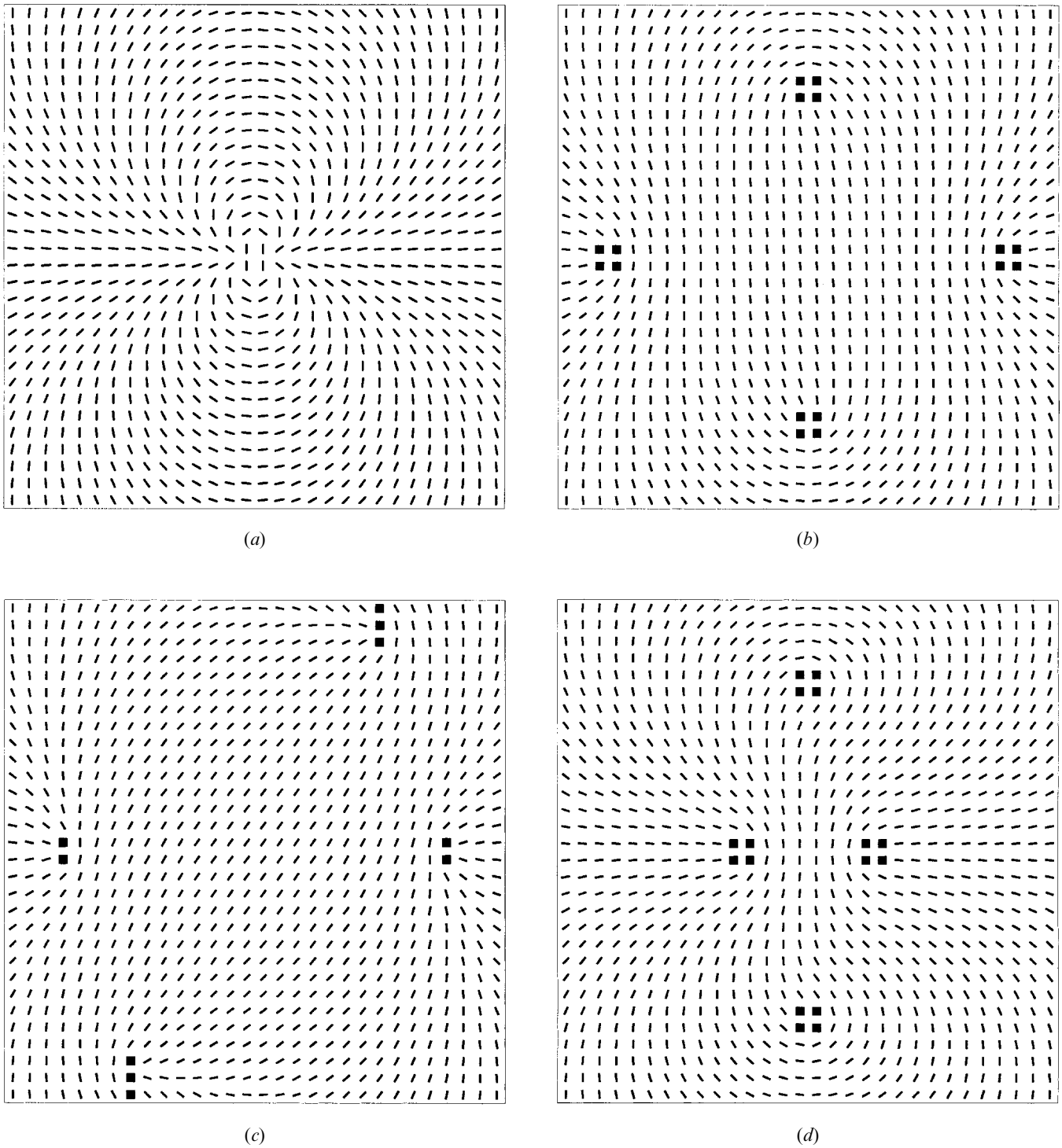

Figure 1. One +2 strength disclination splits into four +1/2 strength disclinations; (*a*) +2 defect; (*b*) $k_1 = k_3$; (*c*) $10k_1 = k_3$; (*d*) $k_1 = 10k_3$. Small filled boxes represent the disclination cores.

pairs remaining, which corresponds to a local free energy minimum. If desired, one can introduce a small magnitude fluctuation to the director field to unlock the 'locked up' state and reach the mono-domain configuration eventually.

As shown in the previous paper [17], the distortion around $+1/2$ defects depended on elastic anisotropy, while the distortion around $-1/2$ defects seemed insensitive to elastic anisotropy. In the following we investigate the splitting of high strength defects.

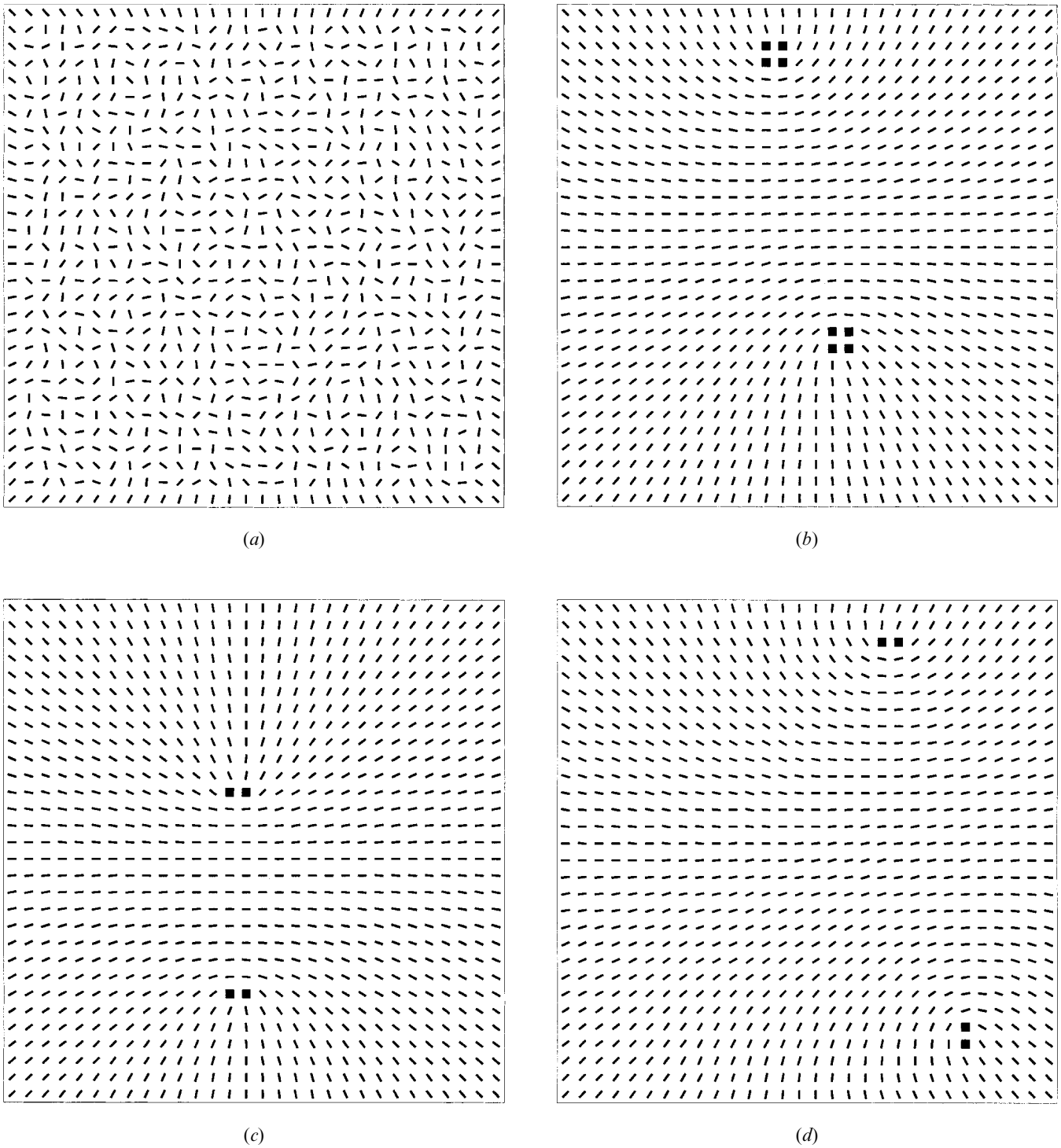

(*a*) (*b*) (*c*) (*d*)

Figure 2. Boundary effects, starting from a pattern randomly oriented and with fixed boundary conditions: (*a*) initial pattern and boundary constrains; (*b*) $k_1 = k_3$; (*c*) $10k_1 = k_3$; (*d*) $k_1 = 10k_3$. Small filled boxes represent the disclination cores.

According to the theory, the elastic free energy of the defects is proportional to the square of their strengths. This makes higher strength disclinations unstable as they have high elastic free energy. A defect of strength half has the lowest free energy, so every high strength defect must ultimately dissociate into half strength singularities. Starting from high strength disclinations, several half strength disclinations can be found at the end of the simulation. Assender and Windle [19] found a difference in the ability to split ± 1 disclinations to $\pm 1/2$ disclinations when different free energy forms were used, in the case of the equal constants, so the energy function form used was significant for the simulation. With fixed boundary conditions, we find that one $s = +2$ defect splits into four $+1/2$ defects in their equilibrium state, as shown in figure 1. In [19], only in the case of the sine-squared relation did the split half defects move apart from each other, leading this expression of the free energy to be the most successful. In the case of equal constants, the current model gives a similar director pattern to that in the case of the sine-squared expression [19], i.e. the split half defects move apart and reach their equilibrium state. Furthermore, figure 1 shows that the shapes of the separated $+1/2$ disclinations depend on elastic anisotropy.

Boundary conditions were found dramatically to affect the final configuration of the director field [19]. If we start with a randomly oriented director field and use fixed boundary conditions defined by a $s = +1$ defect with the core in the centre of the lattice, two $+1/2$ defects remain in the final state, which is its minimum free energy state, as shown in figure 2. We find no half strength disclinations of opposite sign left in the field. Again, the final shapes of the defects are dependent on elastic anisotropy.

4. Disclinations in bulk samples

As mentioned above, the defects generated in 2D are wedge-type disclinations of strength half only. However, the most common defects in bulk samples are disclination lines and loops with a combination of splay, bend and twist distortions in 3D space. These are important for the processing of the LCPs. Whereas it is difficult to reveal the microstructures of line disclinations using the present experimental techniques, the 3D simulation enables us to probe these complex problems.

Disclination lines in the bulk can be described in terms of the angle (α) between the disclination line vector $\mathbf{L}$ and the rotation vector $\mathbf{\Omega}$, about which the director is seen to rotate. The two limiting cases are referred to as pure wedge and pure twist disclinations, for $\alpha = 0$ and 90°, respectively.

We use the topological probes developed previously [14] to identify disclination lines of strength half. In this way, not only the locations of the cores are found, but also the disclination character is distinguished via the angle α between the disclination line and the rotation vector. The following colour coding is used: if α is less than 30°, which implies a predominant wedge type, the colour blue is used; if α is larger than 60°, which implies a predominant twist type, the colour red is used; for the others, i.e. α is between 30° and 60°, which implies a mixed type, the colour green is used. The details have been given by Hobdell and Windle [14].

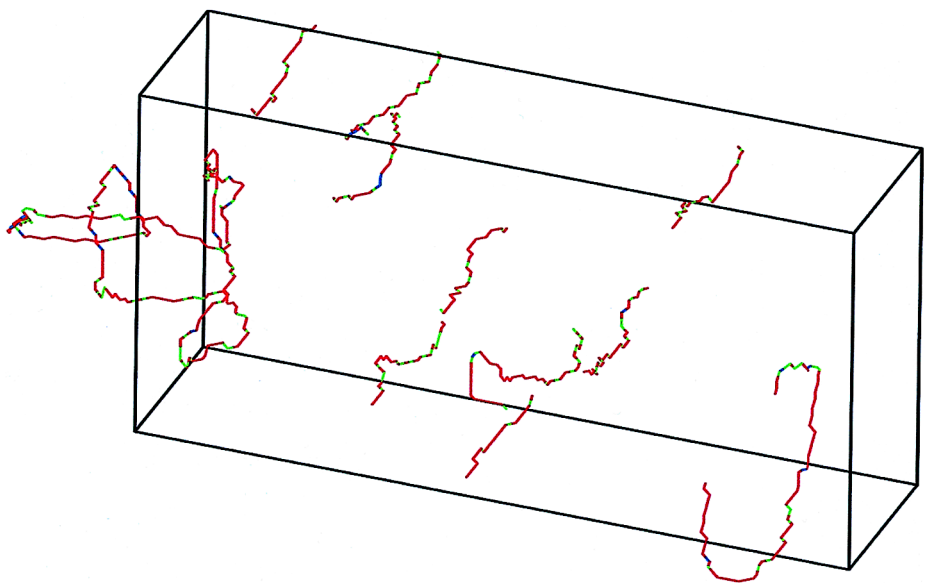

Figure 3. Disclination lines of strength half at time step 5000 from the simulation performed on a $100 \times 50 \times 25$ lattice with periodic boundary conditions in the x and z directions, planar boundary conditions in the y direction and $k_1 = 10k_2 = k_3$.

Disclination lines from the simulations are shown in figures 3–5. The lattice used here is $100 \times 50 \times 25$, planar boundary conditions are used in the y direction and periodic boundary conditions are used in the x and z directions. With periodic boundary conditions, the sample tessellates along the boundaries and the defect lines emerge periodically to form closed loops. For a lower twist constant, for example the value of the twist constant is a tenth of the others, most of the disclination lines are coloured red as shown in figure 3. This means the character of the half strength disclinations is mainly of the twist type. If the bend constant or the splay constant is smaller than the others to a certain degree, the red colour is rare, as shown in figure 4, which indicates

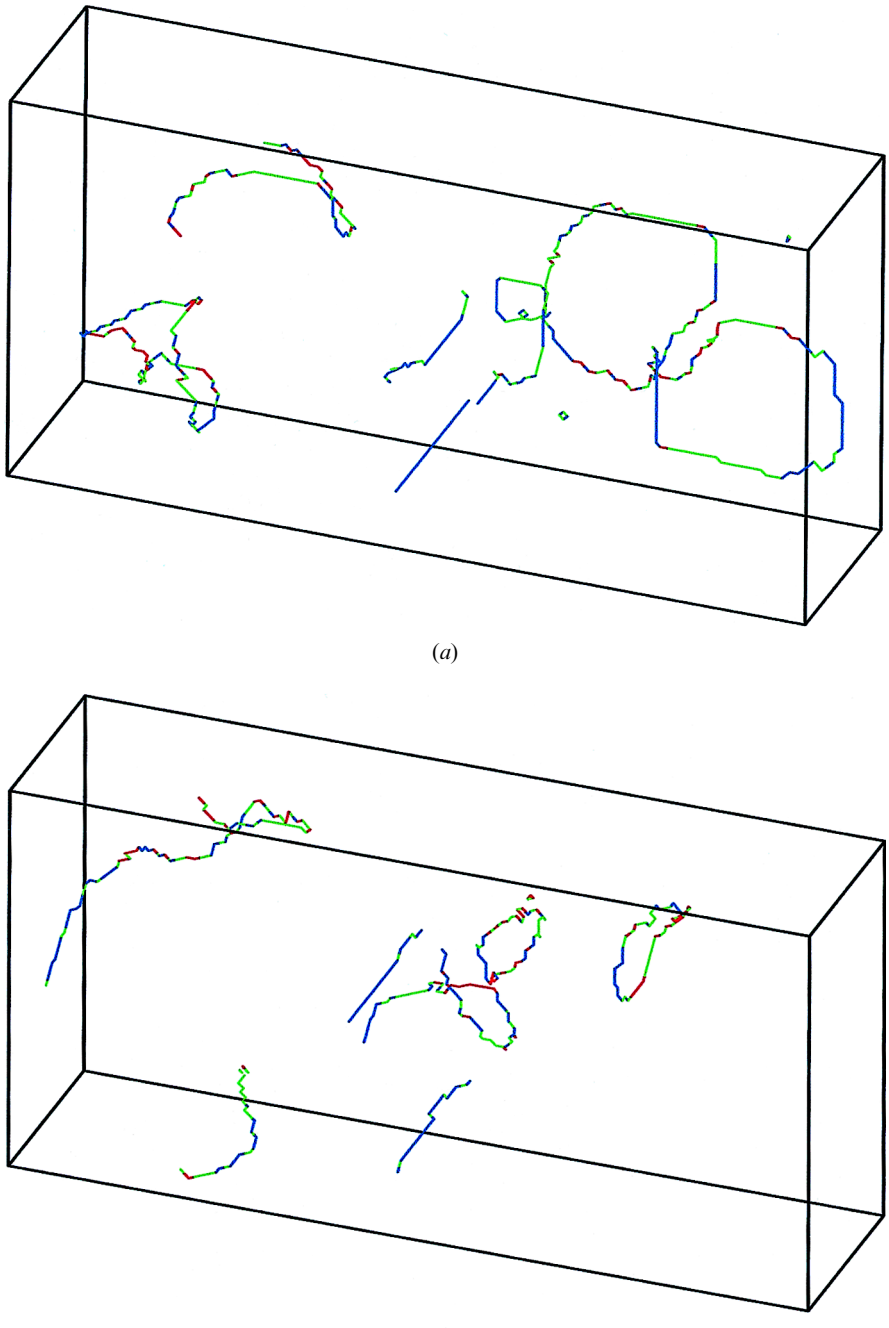

Figure 4. Disclination lines of strength half at time step (*a*) 6000, (*b*) 3000; from the simulation performed on a $100 \times 50 \times 25$ lattice with periodic boundary conditions in the x and z directions and planar boundary conditions in the y direction. (*a*) $10k_1 = k_2 = k_3$, (*b*) $k_1 = k_2 = 10k_3$.

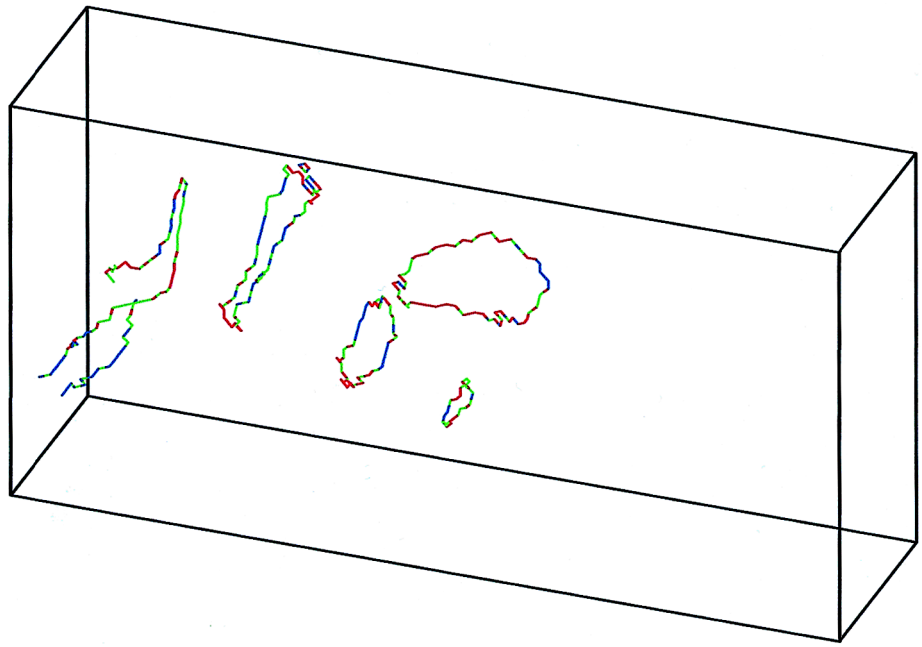

Figure 5. Disclination lines of strength half at time step 900 from the simulation performed on a $100 \times 50 \times 25$ lattice with periodic boundary conditions in the x and z directions, planar boundary conditions in the y direction and with equal elastic constants.

that the character of the half strength disclinations is mainly of the wedge type. This is consistent with the theoretical result of Anisimov and Dzyaloshinskii [11] and the simulation results of the vectorial model [14]. With equal elastic constants, the distribution of the red, green and blue segments of the half strength disclination lines is roughly even. This implies that the character of the half strength disclinations is twist and wedge type balanced, as shown in figure 5. A characteristic of main chain LCPs is that the splay constant is the highest and the twist constant the lowest, so one can expect that disclination lines are rich in the twist type.

The statistical analysis of the distribution of characteristic angles of the disclinations with respect to the above simulations is given in figure 6. It shows that the majority of the disclination lines are of twist character when the twist constant is low, figure 6(*a*); meanwhile most of the disclination lines are of wedge character when the splay or the bend constant is low, figures 6(*b*) and 6(*c*). In the case of equal constants, the distribution of the disclination lines shows no significant variations, figure 6(*d*), but has relatively less wedge character. As explained by Hobdell and Windle [14], this may reflect the following fact: for a given rotation vector $\mathbf{\Omega}$, there are many more possible orientations for the disclination line to be normal to $\mathbf{\Omega}$ than to be parallel to $\mathbf{\Omega}$; consequently the disclination type of twist character might be expected to be the more numerous.

Experiments indicate that integer defects exist without dissociating themselves into half strength defects in the bulk [20]. This has been explained by an escape of the director in the third dimension, which is energetically favourable compared with a planar structure.

For the sake of simplicity, only disclination lines of strength half are visualized in figures 3–5. As well as the half strength disclination lines, escaped $+1$ and -1 disclinations are found in the snapshot of the director fields. The following simulations have been performed on a $30 \times 30 \times 30$ lattice, and periodic boundary conditions are used unless otherwise indicated; the time step is $\Delta t = 0.001$. The nail convention is used in the displays to represent directors pointing out of the page.

With equal elastic constants, escaped -1 disclinations are observed in the bulk. As shown in figure 7, which is a y–z slice at $x = 2$ and time step 400, one escaped -1 disclination and two $+1/2$ disclinations exist in this plane. As explained in [14], this reflects the correct treatment of splay–splay compensation.

If the splay constant is larger than the others, escaped $+1$ disclinations emerge; these avoid splay distortion. Figure 8 is a y–z slice at $x = 23$ and time step 20 000. One escaped $+1$ disclination and two $-1/2$ disclinations emerge in this plane. The distortions around the $+1$ disclination are predominantly of the bend and twist type, manifesting a swirling into the plane. Hobdell and Windle [21] calculated the splay, twist and bend components

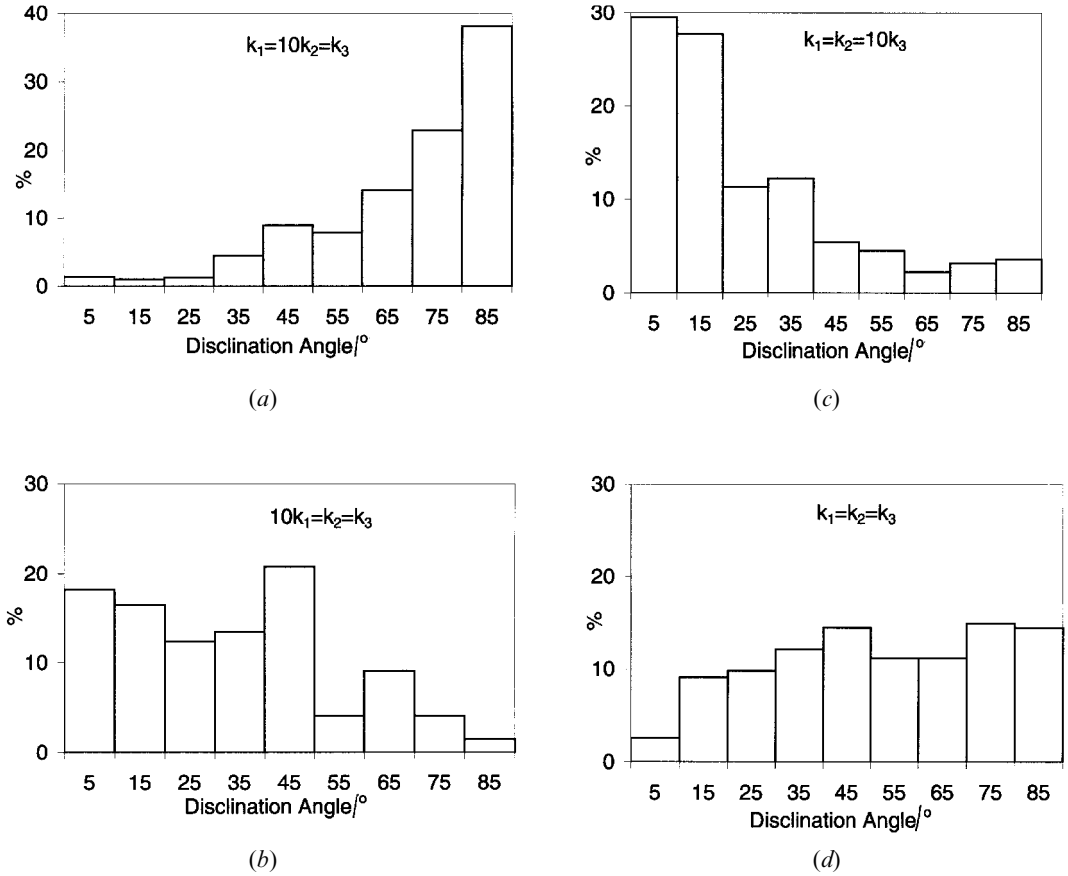

Figure 6. Distribution of the disclination angle for: (*a*) the simulation in figure 3 ($k_1 = 10k_2 = k_3$), the average angle is 71°; (*b*) the simulation in figure 4 (*a*) ($10k_1 = k_2 = k_3$), the average angle is 33°; (*c*) the simulation in figure 4 (*b*) ($k_1 = k_2 = 10k_3$), the average angle is 24°; (*d*) the simulation in figure 5 with equal elastic constants, the average angle is 52°.

of the free energy for several types of point defects, denoted Noeud, Foyer, Centre, Col-foyer and Col. The results showed that the splay component of the free energy had a minimum in the Col-foyer range, the typical configuration of which has tangential character [21]. This indicates that the energetically favoured structure is of tangential type when the splay constant is much larger than the others. The swirling configuration of the +1 disclination found in the present simulation is in good agreement with the results of Hobdell and Windle [21].

If the splay constant is smaller than the others, escaped +1 disclinations of different configuration emerge. Figure 9 is an *x*–*y* slice at $z = 4$ and time step 2500. One escaped +1 disclination and three −1/2 and one +1/2 disclinations exist in this plane. The distortion around the +1 disclination is mostly splay and has a radial shape. According to the result of Hobdell and Windle [21], the twist and bend components of the free energy are zero for the Noeud type point defect. Therefore, in the case of a small splay constant, a +1 disclination tends to form a Noeud configuration to minimize the twist and bend distortions.

5. Summary

Defect structures and annealing of nematics have been simulated using a deterministic tensorial model, starting from an isotropic phase in which the directors are randomly oriented. In 2D, wedge type disclinations of strength half are observed. As expected, the distortions around +1/2 defects depend considerably on elastic anisotropy.

The distortions of the disclination lines of strength half in the bulk also depend on the elastic constants. With a small twist constant, the disclination lines are predominantly of twist type. In contrast, with a large twist constant, the disclination lines are predominantly of wedge type. The disclinations of pure wedge type in 2D can also be viewed as the case of an infinite twist constant.

In the simulation of bulk samples, escaped +1 and −1 disclination lines are found and are accompanied by half strength disclination lines. The integer disclinations, which emerge frequently in the case of equal constants, are −1 disclinations. Escaped +1 disclinations have different geometries that depend mainly on the elastic

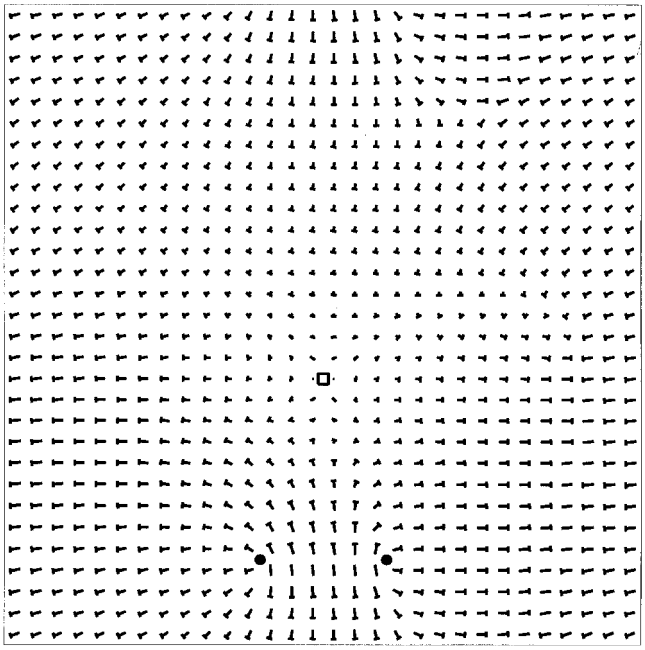

Figure 7. Director distribution at the $x = 2$ plane from the simulation performed on a $30 \times 30 \times 30$ lattice with equal elastic constants and periodic boundary conditions. It shows one escaped -1 disclination and two $+1/2$ disclinations indicated by the small box and filled small circles, respectively.

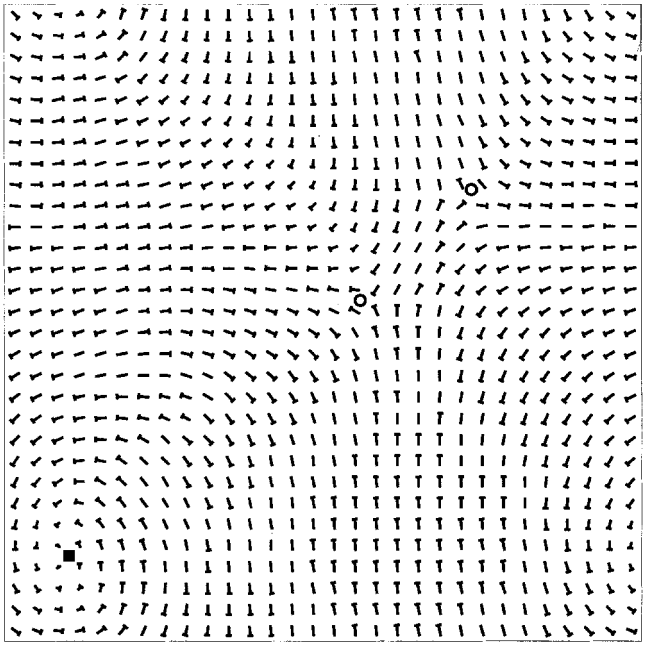

Figure 8. Director distribution at the $x = 23$ plane from the simulation performed on a $30 \times 30 \times 30$ lattice with periodic boundary conditions and $k_1 = 10k_2 = 10k_3$. It shows one escaped $+1$ and two $-1/2$ disclinations indicated by the filled small box and unfilled small circles respectively.

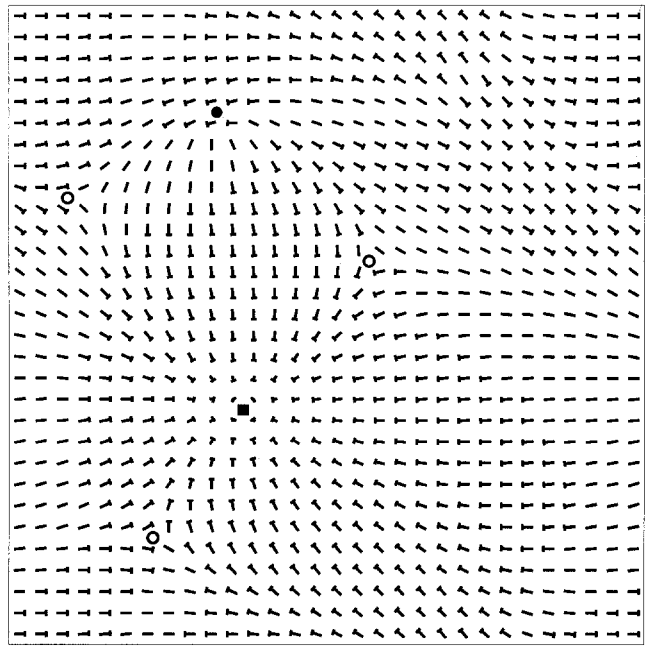

Figure 9. Director distribution at $z = 4$ plane from the simulation performed on a $30 \times 30 \times 30$ lattice with periodic boundary conditions and $10k_1 = k_2 = k_3$. It shows one escaped $+1$, one $+1/2$ and three $-1/2$ disclinations indicated by the filled small box, the filled small circle and the unfilled small circles, respectively.

constants. For example, with a small splay constant, the distortions around escaped $+1$ disclinations are radial in nature; with a large splay constant, they are tangential in nature.

For LCPs, which have a high splay constant and a low twist constant, predominant twist type disclinations are expected in the bulk. This is proposed to be a typical feature of main chain LCPs.

The results reported here are in good agreement with the results of the vectorial model of Hobdell and Windle [14], in which the flip vectorial scheme was used. This confirms that both the flip vectorial model and the current deterministic tensorial model work well in the absence of an external field. The current deterministic model is well suited for investigation of the effect of shear flow on the microstructure of nematics in general and LCPs in particular. The results of such studies are presented separately [22].

The authors would like to acknowledge support by an EPSRC grant under its 'Processing of conventional structural materials' programme.

References

[1] Donald, A. M., and Windle, A. H., 1992, *Liquid Crystalline Polymers* (Cambridge: Cambridge University Press).

[2] Qian, R., Chen, S., and Song, W., 1995, *Macromol. Symp.*, **96,** 27.
[3] Meyer, R. B., 1982, in *Polymer Liquid Crystals*, edited by W. R. Krigbaum, A. Ciferri and R. B. Meyer (Academic Press), Chapter 6, p. 133.
[4] De'Nève, T., Klèman, M., and Navard, P., 1995, *Liq. Cryst.*, **18,** 67.
[5] Chandrasekhar, S., 1992, *Liquid Crystals* (Cambridge: Cambridge University Press).
[6] Thomas, E. L., and Wood, B. A., 1985, *Faraday Discuss. Chem. Soc.*, **79,** 229.
[7] Hudson, S. D., Vezie, D. L., and Thomas, E. L., 1990, *Makromol. Chem., Rapid Commun.*, **11,** 657.
[8] Chen, S., Song, W., Jin, Y., and Qian, R., 1993, *Liq. Cryst.*, **15,** 247.
[9] Hudson, S. E., and Thomas, E. L., 1989, *Phys. Rev. Lett.*, **62,** 1993.
[10] Song, W., Fan, X., Windle, A. H., Chen, S., and Qian, R. (to be published).
[11] Anisimov, S. I., and Dzyaloshinskii, I. E., 1973, *Sov. Phys. JETP*, **36,** 774.
[12] Ranganath, G. S., 1983, *Mol. Cryst. Liq. Cryst.*, **97,** 77.
[13] Gruhn, T., and Hess, S., 1996, *Z. Naturforsch.*, **51a,** 1.
[14] Hobdell, J., and Windle, A. H., 1997, *Liq. Cryst.*, **23,** 157.
[15] Romano, S., 1998, *Int. J. Mod. Phys. B*, **12,** 2305.
[16] Luckhurst, G. R., and Romano, S., 1999, *Liq. Cryst.*, **26,** 871.
[17] Tu, H., Goldbeck-Wood, G., and Windle, A. H., 2001, *Phys. Rev. E*, **64,** 011704.
[18] Chuang, I., Yurke, B., Pargellis, A. N., and Turok, N., 1993, *Phys. Rev. E*, **47,** 3343.
[19] Assender, H. E., and Windle, A. H., 1994, *Macromolecules*, **27,** 3439.
[20] Cladis, P. E., 1972, *J. de Physique*, **33,** 591.
[21] Hobdell, J., and Windle, A. H., 1995, *Liq. Cryst.*, **19,** 401.
[22] Tu, H., Goldbeck-Wood, G., and Windle, A. H., 2002, *Liq. Cryst.*, **29,** 335.